Magnetoteluric Study in the Region De Los Lagos to Study Volcano-Tectonic Processes in the Southern Andes

Maria Jose Segovia Baldovino (masegovia@ug.uchile.cl)
Universidad de Chile Facultad de Ciencias Fisicas y Matematicas https://orcid.org/0000-0001-7399-8199

Daniel Diaz Alvarado
Universidad de Chile Facultad de Ciencias Fisicas y Matematicas

Katarzyna Slezak
Universidad de Chile Facultad de Ciencias Fisicas y Matematicas

Felipe Zuñiga Armijo
Universidad de Chile Facultad de Ciencias Fisicas y Matematicas

Full paper

Keywords: tectonic, magmatic, Electrical, Serpentinization

Posted Date: August 28th, 2020

DOI: https://doi.org/10.21203/rs.3.rs-63052/v1

Version of Record: A version of this preprint was published on January 4th, 2021. See the published version at https://doi.org/10.1186/s40623-020-01332-w.

Abstract

In order to analyze the process of subduction of the Nazca and South American plates in the area of the Southern Andes, and its relationship with the tectonic and volcanic regime of the place, magnetotelluric measurements were made through a transversal profile of the Chilean continental margin. The data processing stage included the analysis of dimensional parameters, which as first results showed a three-dimensional environment for periods less than 1s and two-dimensional for periods greater than 10s. In addition, through the geomagnetic transfer function (tipper), the presence of structural electrical anisotropy was identified in the data. After the dimensional analysis, a deep electrical resistivity image was obtained by inverting a 2D and a 3D model. Surface conductive anomalies were obtained beneath the central depression related to the early dehydration of the slab and the serpentinization process of the mantle that coincides in location with a discontinuity in the electrical resistivity of a regional body that we identified as the Nazca plate. A shallow conductive body was located around the Calbuco volcano and was correlated with a magmatic chamber or reservoir which in turn appears to be connected to the Liquiñe Ofqui fault system and the Andean Transverse Fault system. In addition to the serpentinization process, when the oceanic crust reaches a depth of 80-100km, the ascending fluids produced by the dehydration and phase changes of the minerals present in the oceanic plate produce basaltic melts in the wedge of the subcontinental mantle that give rise to an eclogitization process and this explains a large conductivity anomaly present beneath the main mountain range.

Key Points

Electrical resistivity images of the Los Lagos region, Chile.

Two and three dimensional model of the electrical resistivity structure of the Southen Andes subduction zone (41°S).

Processes of generation, migration and accumulation of fluids.

Serpentinization and eclogitization processes

1 Introduction

The Southern Andes constitute an orogenic mountain belt developed on an active continental margin, with subduction between the Nazca and South American tectonic plates as the main cause of the magmatic and tectonic processes in the area (Hervé, 1994). The area of study is framed in the Southern Volcanic Zone of the Andes (SVZ), in this zone, the complex interaction between tectonic and magmatic processes is evident in the architecture and geochemical signature of the volcanic systems, Cembrano & Lara (2009) relate this spatial distribution of plutons, dikes and volcanic cones, with the lithospheric stress generated by the Liquiñe Ofqui Fault System. The Liquiñe Ofqui Fault Zone (LOFZ) corresponds to a strike-slip system of approximately 1200 km long, where most of the seismic activity of the continental crust in the South of Chile is concentrated (Lavenu & Cembrano, 1999). The South of Chile represents an

attractive place for a volcano-tectonic study; since it is located in an orogenic margin, with an important system of faults dominating the terrestrial crust and active volcanic centers, it appears as a favorable environment for the development of natural disasters related to volcanoes and earthquakes. Arc volcanism and seismic activity are closely related to the distribution of fluids from physical-chemical processes that occur in subduction (Saffer, 2017).

The process of generating magmatic fluids that migrate through the continental crust depends on some physical parameters of the oceanic plate such as its composition, thickness, angle of inclination with which it subducts and its degree of hydration, which in turn depends on the age and porosity of the plate (Völker & Stipp, 2015). As the oceanic slab subduces the continental slab, due to the increase of temperature and pressure conditions, mineralogical changes are generated as a result of the dehydration of the Nazca plate. One of the most significant processes corresponds to the serpentinization process of the mantle, in which a metamorphic alteration is produced that affects the ultramafic rocks of the upper mantle. In seismic studies, the serpentinization zones can be observed as zones where the seismic velocity of S wave and the density of the mantle is drastically reduced (Hyndman & Peacock, 2003). Serpentinization can also generate seismic reflectivity, increased magnetization and a reduction in mechanical strength (Hyndman & Peacock, 2003). The other important process corresponds to eclogitization that occurs at greater depths where the temperature and pressure conditions are extreme, in this process all the remaining water present in the slab forming minerals is released (Leech, 2001). The serpentined and eclogitized zones are clearly shown in seismic tomography and in resistivity images measured with the magnetotelluric method. Examples of works where these processes can be identified by geophysical methods are those of Reynard, et al. (2011), Navarro (2019), Evans, et al. (2014), Wannamaker, et al. (2014), Kapinos, et al. (2016) and Cordell, et al. (2019).

As the oceanic slab dehydrates, through processes of serpentinization and eclogitization, fluids are generated that rise and fall the point of function of the continental crustal rock, forming magmatic fluids that migrate and control the creation of volcanoes in the arcs. These fluids can be transported through fault networks to the surface of the Earth (Clemens & Mawer, 1992). Therefore, the stress of the lithosphere influences the spatial distribution of plutons, dikes and volcanic cones.

The magnetotelluric method is useful in the study of the above processes because the conductivity of the crust and mantle rocks increases with the presence of fluids, and it is one of the few geophysical methods that can penetrate to the depths at which these processes are generated.

The present work seeks to study the lithospheric structure of electrical resistivity in the Southern Andes to analyze processes of generation, migration and accumulation of fluids related to the subduction between the Nazca and South American plates in the Chilean continental margin.

2 Geological Setting

The oceanic Nazca plate subducts beneath the continental South American plate along the Andes with a convergence rate of 6.6.cm/year and an azimuth of 77° (Angermann, et al., 1999). In the Lake District

between 33° and 46° south latitude, the Nazca plate has a subduction inclination of ~ 20° (Tassara & Echaurren, 2012). The stretch of oceanic plate between 40°S and 41.5°S has an age of 17.3 Ma (Völker & Stipp, 2015).

In Fig. 1, from West to East, the main morphological units are given by The Coastal Range, south of 38°S, which is an accretionary prism metamorphosed in late Paleozoic to late Triassic times (Thomson & Hervé, 2002). The eastern flank of the Coastal Range is characterized by intrusive and volcanic-sedimentary Mesozoic sequences suggesting the eastward migration of the volcanic arc from the Jurassic; The Depression or Central Valley, which constitutes the extension of the Osorno-Llanquihue basin towards the south, contains approximately 4 km of Cenozoic marine volcanic rocks and glacial sediments in a 70 km wide depocenter parallel to the trench (Jordan, et al., 2001); The eastern limit of the Central Depression is defined by the North Patagonian Batolito and the current Volcanic Arc in the Northern Patagonian Andes, where the Liquiñe Ofqui Fault Zone is developed. The Batolito is 2000 km long and 200 km wide, it is composed mainly of plutonic alkaline rocks from the Middle Jurassic to the Miocene (Glodny, et al., 2008). The main water bodies in the study area are the lakes of glacial origin, Llanquihue Lake (L.LL) and Todos Los Santos Lake (L.TS).In the Southern Volcanic Zone of the Andes, cortical level structures related to the LOFZ and Andean Transverse Fault (ATF) have been identified. The oblique convergence between the Nazca and South American plates is the main cause of the transpressive dextral deformation in the Earth's crust, dominated by the sliding of regional to local scale by these fracture networks.

The LOFZ is associated with a dextral transpressive regime from at least the last 6 Ma (Cembrano, et al., 1996), extending from the town of Liquiñe (39°S) to the isthmus of Ofqui (47°S). At latitude 41°S, Lavenu & Cembrano (1999) attribute a vertical geometry to the fault line, generated by dextral transpressive systems of N-S orientation, with double vergence, developed between the Neogene and Quaternary. The LOFZ is characterized by sub-vertical NNE oriented master segments and transstensional faults from ENE to EW (Cembrano & Hervé, 1993).

Most, if not all, of the volcanic systems at the top of the LOFZ are monogenetic, suggesting that they were formed by geologically instantaneous events.

Another important fault system to highlight in the Southern Volcanic Zone corresponds to the Andean Transverse Fault, these include a series of NW oriented faults, probably inherited from a pre-Andean architecture with inverse synestral kinematics and local reactivation of normal sliding (Radic, 2010). It is suggested that the ATF is older, dating from the pre-Andean, or equivalent to the LOFZ (Pankhurst, et al., 2006).

Fracture networks or faults in the continental crust have been considered as an efficient route through which fluids are transported to the earth's surface (Clemens & Mawer, 1992). Therefore, the lithospheric stress influences the spatial distribution of plutons, dikes and volcanic cones. However, crustal deformation not only plays an important role in magma migration. More importantly, it can exert

fundamental control over magma-differentiation processes which, in turn, can determine the nature and composition of volcanism along continental margins.

The volcanic zone of the Southern Andes, is located between 33 ° S and 46 ° S. The complex interaction between tectonic and magmatic processes is evidenced by both the architecture and the geochemical signature of the volcanic buildings in this zone. Throughout the SVZ strike, variations in the composition of the products of the volcanoes and in their orientation are evident. The structures of NE-SW orientation and originating mostly from primitive magmas belong to stratovolcanoes and monogenetic cones associated to LOFZ guidelines while stratovolcanoes of WNW orientation and with compositional products from basaltic to rhyolithic rocks are associated to structures of the ATF (Cembrano & Lara, 2009). The main factors that explain the variations along the strike in the nature and composition of volcanism are the variation in crust thickness, the source of magma, the lithospheric nature and structure and the existence of a predominant intra-arc fault system (Cembrano & Lara, 2009). The thickness of the crust below the volcanic arc is approximately 50 km at latitude 33°S and decreases towards the South, reaching a thickness of 35 km at 46°S (Tassara & Yañez, 2003).

One of the most important volcanoes for its activity in the area corresponds to the Calbuco volcano (2,003 m.a.s.l.), it is built on a base of Miocene granite and meta-sedimentary mafic igneous rocks of the Upper Paleozoic and, unlike most of the volcanoes of the Southern Andes, it is located west of the main route of the Liquiñe-Ofqui Fault Zone, and is not clearly related to or controlled by regional structures. Its documented historical activity includes at least 12 eruptive cycles, 4 of which in the 20th century included effusive and explosive activity. The highly hydrated magmas that characterize the volcano's petrology increase its potential to generate explosive eruptions. The main hazards are associated with the volcano, however, there are the evidences of lahars and block and ash flows, mainly directed towards the fans to the Northeast, South and Southeast, in areas with growing population and infrastructure development (Selles & Moreno, 2011). In April 2015 the last volcanic eruption of the Calbuco was recorded. According to studies such as Castruccio, et al. (2016), the erupted products were mainly basaltic andesite. Another important volcanic structure to mention in our study area corresponds to the Osorno Volcano stratum belonging to the Middle Pleistocene (< ca. 200 ka). Together with the La Picada, Puntiagudo and Cordón Cenizos volcanoes, it forms a transversal volcanic chain of N60ºE orientation. The eruptions of the central crater, Osorno volcano, have generated basaltic pyroclastic flows and tephras of dacitic composition that date from the Holocene (< 10 ka) and are distributed in a wide sector around the volcano. The historical eruptive activity of the Osorno volcano has been essentially characterized by low explosive episodes among which the fisural eruption of 1835 AD stands out. (Moreno, et al., 2010)

Other volcanic centers in our study zone correspond to the Puntiagudo stratovolcano (2493 m.a.s.l.) that within its volcanic materials stand out the lava emissions and pyroclastic and laharic deposits of predominant basaltic composition and the Tronador volcano that corresponds to a mixed stratovolcano that houses a great glacier on its summit that plays a great role in the violent interaction between magma and water generating explosive reactions. (Mella, et al., 2005).

3 Methods

3.1 Magnetotelluric data

Magnetotellurics (MT) is an electromagnetic method of geophysical exploration used to deduce the electrical resistivity structure of the Earth at depths ranging from tens of meters to hundreds of kilometers. This method uses a source signal of external origin, natural variations of electric and magnetic fields of the Earth, generated by physical processes such as solar variations and magnetic storms. The spectra of these variations cover periods ranging from 10^{-3} to 10^{5} [s] and are generated by the interaction between the solar wind, the magnetosphere and the ionosphere of planet Earth (Vozoff, 1991).

The MT method is based on the simultaneous measurement of the total electromagnetic field, i.e. the time variation of the magnetic field B(t) and the induced electric field E(t). The electrical properties of the underlying material can be determined from the relationship between the components of the measured variations of electric (E) and magnetic (B) fields, or transfer functions: the horizontal electric (Ex and Ey) and the horizontal magnetic (Bx and By) and vertical (Bz) field components. The transfer functions consist of a complex impedance tensor which relates the measured electric field components to the magnetic field components and a geomagnetic transfer function which is often called a tipper and relates the horizontal magnetic field components to the vertical magnetic field component. In general the resistivity structure of the earth is three-dimensional obtaining an impedance tensor of four components, complex impedance tensor, however, if it is a two-dimensional structure where the resistivity does not vary along the geoelectric strike the diagonal components of the tensor are null as long as the coordinate system is parallel to the strike direction. In this case the two surviving tensor components are related to two independent modes, the magnetic transverse (TM) and the electric transverse (TE). Sometimes if the strike preference angle is known, the tensor can be rotated so that the diagonal components are minimized. Generally the elements of the impedance tensor can be plotted as apparent resistivity and phase as a function of period (reciprocal of frequency), these graphs can give us an idea of variations in the average resistivity of the medium that has been measured so that short periods are related to shallow depths and long periods to greater depths. Some components of the measured electric fields can be affected by a phenomenon called Static Shift that is generated due to shallow conductive structures, or due to the effect of topography and is observable in a delay at the beginning of the apparent resistivity curves that in ideal conditions should start at the same value. On the other hand, the geomagnetic transfer function serves to identify lateral resistivity contrasts and can be represented as arrows or induction vectors, under the convention of Wiese (1962) the vectors point in the opposite direction to the conducting body. When making long period measurements near the ocean it is expected to observe the so-called shore effect on the induction vectors for long periods, due to the large resistivity contrast between the ocean and the continent the orientation of the vectors over longer periods should be expected to be in the opposite direction and perpendicular to the shore.

In order to obtain a lithospheric model of the electrical resistivity structure of the study area, several field campaigns were carried out between December 2018 and April 2019, where 14 long-period and 10 broadband stations were installed along the profile transverse to the coast (fig1). Three types of stations were used to carry out the measurements, ADU (Analog/Digital Signal Conditioning Unid), NIMS (Narod Intelligent Magnetotelluric Systems) and Lemi417. All stations were oriented with a geomagnetic coordinate system. The data processing included the application of filters to the obtained time signals to eliminate noise signals where possible, remote reference application in some cases to improve the data quality of the stations that were measuring simultaneously. The signals obtained with ADU stations were processed with the robust process developed by Egbert & Booker (1986), those obtained from NIMS stations were processed with the code developed by Egbert & Livelybrooks (1996) and the signal obtained with Lemi stations were processed with the robust code developed by Egbert (1997).

We proceeded to calculate the strike in period intervals for all stations with the code developed by Smith (1995) in order to know if there was any preferential direction of the structure and to diagnose a two-dimensional space. In figure 2 it can be seen that for the range of periods between 10^{-3}s and 10^{0}s the structure does not have a preferential orientation, evidencing a three-dimensional environment, while for periods greater than 1s the structure begins to behave two-dimensionally. In figure 3 the induction vectors are plotted in a length vs period profile where we can observe characteristic behaviors of areas where we expect to find conductive bodies in the inversion models. The small magnitude of the arrows enclosed by the dotted celestial line and the W-E direction of the arrows enclosed by the purple line suggests a conductive zone towards the west of the Llanquihue lake, the direction of the vectors enclosed by the pink dotted line could be indicating the presence of a conductive body around the Osorno Volcano, while the magnitude of the arrows enclosed by the green dotted line indicates the presence of a body of low resistivity in the Andes mountain range.

For long periods (>10^{1}s), the arrows were expected to have a regional behaviour in W-E direction due to the coast effect, however, it can be observed in the vectors delimited by the yellow dotted line that have a SW-NE direction. This behavior of the vectors is studied by Brasse, et al. (2009) in the Chilean continental margin, between latitudes 38°-41°S and attributes it to the resultant between the effect of the ocean and the presence of a layer with structural electrical anisotropy in the crust.

An electrically anisotropic medium can be, for example, a space influenced by micro-scale hydrated faults that can become a macro-scale structure if these structures have a preferential general orientation. From the above, it can be inferred that one way to mitigate the effect of anisotropy on the data is to work with the periods between 10^{1}s and 10^{3}s, since this range has a general preferential strike (Martí, 2014)

3.2 Magnetotelluric data inversion

We carried out 2D and 3D inversions in order to obtain a realistic model that is close to the geology of the region. In addition, Martí (2014) recommends testing different inversion software, different models and

altering different parameters in the inversions until we obtain models without artifacts resulting from structural electrical anisotropy.

For the two-dimensional inversion we used the WinGlink software that uses the 2D inversion code from Rodi & Mackie (2001) , this algorithm minimizes an objective function, by means of the non-linear conjugate gradient method (NLCG), which penalizes the differences between the data and the model response, also condemning the second spatial drifts of the resistivity model, in order to obtain a contrast of resistivities in a smooth model. Taking into account the dimensional analysis performed previously, the data set was chosen between the range of periods 10^1s and 10^3s, taking into account that anisotropy is mostly reflected in the induction vectors, it was chosen to model only the TE and TM mode data. Background resistivities of 100 and 500 Ω.m were tested, the minimum frequency used was 0.00008hz, error floors was set to 20% for apparent resistivities and 5% for phases. A fine grid with growth factor 1.2 was used in depth and to the sides of each station (see fig 4 a). Although, the topography option was activated, it is not influential in the inversion when working with long period data.

To the inversion a priori known information of the zone was delivered, an ocean was drawn with a resistivity of 0.3Ωm and a mean depth of 5km according to the bathymetry registered by the National Oceanic and Atmospheric Administration (www.ngdc.noaa.gov/mgg/topo/topo.html).

From the analysis of results of synthetic data modeling and the comparison between 3D and 2D inversion results, Chang-Hong, et al. (2011) the possibility of obtaining a true 3D resistivity structure from 2D profile data was demonstrated. Furthermore, our results show that not only a reasonable three-dimensional image can be obtained under the 2D profile but also 3D structures close to the profile that cannot be obtained with a two-dimensional inversion are achievable, provided that the four elements of the impedance tensor and the tipper are modeled, since the elements of the diagonal have a special effect on the recovery of the distribution of three-dimensional anomalies close to the profile..

There are several MT studies, which deliver 3D models from data collected along a 2D profile, for example, Meqbel, et al. (2016), Patro & Egbert (2011) and Beka, et al. (2016).

For the three-dimensional model, a logarithmic grid was designed according to the order of periods and the maximum depth expected to be reached with each set of data. The growth factor in x and y direction was set at 1.3 while 1.2 was chosen for the depth.

A total of 52 frequencies were used for the impedance tensor and 50 frequencies for the tipper. The smoothing factor was set at 0.7. The floor error for the diagonal components was 7%, while for the components outside the diagonal and the tipper 5%. For this model the bathymetry of the Pacific Ocean was taken into account, this was downloaded from the National Oceanic and Atmospheric Administration and with an electrical resistivity defined at 0.3Ωm.

Tests were performed including and excluding the Nazca plate in the 2D and 3D grids of the a priori models, the Nazca plate was drawn as a layer of 9.000Ωm resistivity with the depths indicated in the

study by Tassara & Echaurren (2012) that presents a model of the depth of the Slab, the continental moho and the contact between lithosphere and asthenosphere in our study zone. We observed that the bodies generated in each case were similar in location, magnitude and shape, however we obtained better RMS in the models that did not include the Nazca plate.

Finally, we performed sensitivity analyses in both models obtained in order to validate the need of each body within the model for the final fit of the curves of each station.

The sensitivity analysis consists of eliminating the structure and studying the response of the model through forward modeling. The response of the new model is compared with the response of the original model to analyze how it is modified when a body is removed. If the variation influences different stations and the size and distance to the location of the body is consistent with the perceived fluctuation in the curves of each site, it can be concluded that the body is necessary for the fit of the observed data.

4 Result

The two-dimensional model (Fig. 5) was fitted with an RMS of 1.88% after 200 iterations. In it, several conductive and resistive bodies can be observed that can be roughly related to the known geology and tectonics of the zone. In Fig. 5, the resistive body R1, with values between 1,000 and 8.000Ωm, is intrinsically related to the subducting Nazca plate; it must be taken into account that the plate has an important resistivity decrease at 50 km depth. R2, on the other hand, is a highly resistive body, located under the Osorno Volcano and between the Llanquihue and Todos Los Santos lakes. It is located within the continental crust, from a shallow depth to ~ 20 km. Conductive "C" bodies are often related to fluids, hot zones, salt - water bodies, etc. Towards the west of the profile, in the central depression, two conductive bodies appear, shallow C1 and C2 and with resistivity of 1 and 7Ωm respectively. Towards the east of the profile, near the Tronador volcano, a body "C3" is observed that crosses the earth's crust, from the mantle, with a resistivity of between 13 and 50Ωm. In magnetotellurics, broadband data has better resolution for shallow depths while long period data has better resolution for greater depths. Although the present work inverted models with both broadband and long period data, it should be noted that the periods used for broadband stations were $\geq 10^{1}$s, so it is not expected to obtain high resolution of the surface bodies. For the interpretation of results, the existence of equivalent models that will deliver the same data fit, but with a completely different body distribution, should also be considered. For example, a small conductive body could be equivalent to a body with lower conductivity, but larger size.

It is believed that the seismicity in the South of Chile is quite lower, compared to the seismicity rate of the rest of the country, several authors such as Agurto-Detzel, et al. (2014) and Lange et al., (2008), affirm that the seismicity of this zone is dominated mainly by the Liquiñe Ofqui fault system. By plotting the seismicity registered since 2013 in our electrical resistivity image, it is easy to notice the accommodation of the earthquakes in the subduction zone and in the zone where the fault system is believed to cross the latitude of the profile.

Figure 5a shows three depth cuts parallel to the station profile (located in Fig. 5b). In this model different conductive and resistive bodies can be seen below and outside the profile. There is a good correlation with the bodies "C" and "R" generated by the 2D inversion with the bodies generated by the 3D inversion being C5, C6 and C7 three conductive bodies that only appear in the 3D, this could be due to the fact that in the two-dimensional model the value of the resistive R2 is very high and fades the resistivity value of these bodies. The reason why some bodies are shown in the 2D inversion, even when they are outside the profile, according to the 3D model, may be due to a high resistivity contrast between these bodies and the resistivity below the stations, for example, C1 and C2.

It is also possible that the location of the bodies outside the profile in the 3D model is related to the influence of the tipper that was discarded in the 2D inversion due to structural electrical anisotropy. However, there are studies such as the one by Slezak, et al. (2016), located in the Northwest of Poland where, without having evidence of structural electrical anisotropy in the crust, they obtain in the 3D model conductive bodies outside the profile that are not evident in the 2D model.

The model we chose to interpret and discuss corresponds to the 3D model, with a RMS 1.95%, because it covers all the bodies shown in the 2D model and additionally provides other bodies that converge well with the geology of the zone. The three-dimensional model was obtained with all the available information from the impedance tensor and tipper.

5 Discussion

R1 has been identified as a regional body at great depths related to the Nazca plate that subduces under the South American plate and its decrease in resistivity at 50 km depth is related to the process of serpentinization by an early dehydration of the Slab, this serpentinization of the mantle produces an increase in porosity that leads to a decrease in electrical resistivity, which can be further reduced by the production of electrically conductive magnetite networks (Stesky & Brace, 1973). The Nazca plate has been determined by several long term magnetotelluric studies, in the South Central and Southern zone of Chile, for example, Brasse, et al. (2009), Kapinos, et al. (2016) and Cordell, et al. (2019). On the other hand, Worzewski, et al. (2011) with a study of MT in Central America where the Nazca, Cocos and Caribbean plates interact observe this important decrease in resistivity in the same zone where DeShon, et al. (2006) they observe a decrease in the S wave velocities, both studies propose that this is a zone of serpentinization of the mantle.

Below the Central Valley, conductive anomalies formed by bodies C1 and C2 are located superficially in the crust, just above where the Nazca plate discontinuity appears. In the three-dimensional model (see central profile), body C2 seems to migrate from the mantle. Geologically, we relate these bodies to the early dehydration of the Slab, in this process, water bound to the pores is expelled from the subducting slab to shallow depths by compaction and lithitization (Hyndman, et al., 1997).

The result of a seismic profile located a few meters from our magnetotelluric profile in the zone of the Central Valley, studied by Jordan, et al. (2001), shows some seismic reflectors in the zone where bodies

C1 and C2 are observed that relate to faults at a depth not greater than 10 km, we could affirm that these faults are facilitating the migration and distribution of fluids in the central valley.

The C3 anomaly can be interpreted as a zone of fluid accumulation resulting from a partial fusion related to the Nazca plate serpentinization or eclogitization process and high pressure and temperature conditions at depth. Numerical models by Völker & Stipp (2015) suggest that approximately 50% of the water intake fluids from the crust and mantle are released in the front arc or rear arc, this could explain why the C3 conductor is much larger than the other conductors and why it is located more to the east of the profile. This important conductivity anomaly is comparable to anomalies found in studies conducted in other zones that have developed typical surface expressions such as volcanic arcs around the world, e.g., magnetotelluric studies in British Columbia (Soyer & Unsworth, 2006), in Oregon (Cascadia) (Jiracek & Curtis, 1989), in Mexico (Jödicke, et al, 2006), in Northern Chile (Schwalenberg, et al., 2002) and (Brasse, et al., 2002), in Greece (Galanopoulos, et al., 2005), in Japan (Nankai) (Ichiki, et al, 2000) and (Ryukyu Trench) (Shimakawa & Honkura, 1991), in Costa Rica (Worzewski, et al., 2011), in Central and Southern Chile (Cordell, et al., 2019), (Brasse, et al., 2009) and (Kapinos, et al., 2016)

The C5 body with resistivities around 1Ωm located north of the Osorno volcano at a depth less than 10 km could be related to an active magmatic and/or hydrothermal system associated with the volcano, its such low resistivity values correlate well with a conductive zone of molten mass accumulation. The report of volcanic activity in the Los Lagos region (SERNAGEOMIN, n.d.) has recorded multiple seismic activity between 2017 and 2019, related to the Osorno volcano; Most of the seismic events have been located towards the Northwest of the volcano at depths of less than 10 km, coinciding with the location of the anomaly, however, it must be clarified that the location of the events it provides is not exact, also, taking into account that the last episode related to a volcanic eruption of the Osorno dates from the year 1835 and that the information of the reports is not sufficient either to analyze the focal mechanisms and to confirm that the events are own of the volcano, we can affirm then that these events are attributed to the System of Fallas Liquiñe Ofqui. An important consideration relates to the effect of including or excluding topography in inversion algorithms. For the Merapi volcano, located in Indonesia, Müller & Haak (2004) they show that the induction vectors suggest a conductive structure centered in the volcano that they attribute to the high topography of its cone, that is, in these cases special care must be taken to differentiate how much of the response of the induction vector is due to the topography and how much to the conductivity of the rock. Brasse & Eydam (2008) also analyze the topographic effect on volcanic buildings with a high slope, finding that the inversions create artifacts related to a static displacement in the electric field resulting from the effect of the topography. According to the above and knowing that in the 2D and 3D models of our study the topography was not included, it is very likely that C5 is simply an artifact created by the inversion software as an effect of the topography of the cone of the Osorno volcano.

The anomaly named C6, located to the east of the Osorno volcano, coincides with the location of the Liquiñe Ofqui fault zone at 72.28°W in length. The elongated shape of this body supports well the idea that it is a fluid ascent facilitation conduit due to a fractured weakness zone related to the fault system.

The papers by Cembrano & Lara (2009) and Perez-Florez, et al. (2017) confirm that transverse strike-slip faults are oriented favorably with respect to the stress field and promote vertical migration of magma. It should be noted that the C6 body, in our model, does not present resolution for depths greater than 20 km. This trace of the fault is also observed in the study of Zuñiga Armijo (2019), by means of broadband magnetotelluric measurements, Zuñiga Armijo (2019) proposes that this fault is facilitating the ascent of fluids towards a mush type reservoir of the Osorno volcano.

The C7 anomaly shown in the three-dimensional inversion is a conductive body, located under Calbuco volcano that could be interpreted as a magmatic reservoir of depth between 10 and 20 km that is connected to a conduit or structure of the Andean transverse faults and that is directed towards the trace of the Liquiñe Ofqui fault.

According to Selles & Moreno (2011) the Calbuco volcano, does not present evidence of being located on an important regional structure, however, Perez-Florez, et al. (2017) outline some guidelines of the Andean Transverse Fault system, which present orientation NOT located in the southern volcanic zone of the Andes.

Morgado, et al. (2019) through a petrochemical study of samples from the Calbuco eruption in 2015, propose the existence of a mush type deposit, located in the upper crust up to 5.5–9.5 km deep. Delgado, et al. (2017) suggest a pressurized flattened spheroid shape for the reservoir below the Calbuco volcano through modeling of the co-eruptive subsidence signal. Considering the 2015 lava flows, Morgado, et al. (2019) restricted the pre-eruptive conditions to: temperature 900–1060 °C, pressure 2–6 kbar, 2–4% H_2O and a variable amount of SiO_2 between 55.6 and 56.9%. Castruccio, et al. (2016) calculated SiO_2 between 54–55 wt% and Na_2O between 3.6–3.8%, 4–5% H_2O and pressures of 180–240 MPa.

Using the SIGMELTS web application (Pommier & Le-Trong, 2011) a model is built with the above parameters, estimating an electrical resistivity of the variable magmatic reservoir between 2–10 Ωm, which could be an indicator that, by model equivalence, our C7 anomaly is less deep and more conductive.

There is a difference in the composition of the products in the two volcanoes, the Osorno is predominantly basaltic while the Calbuco is andesitic. However, ground, petrographic and geochemical observations suggest that the andesitic composition of the Calbuco is the result of a contamination of subcortical basaltic magmas with magmas generated at the cortical level (Lopez-Escobar, et al., 1992). Thus, the difference between the composition of the Osorno and Calbuco products could be explained by an apparent differentiation of the magma that has to travel a greater distance to reach the volcanic reservoir, or perhaps it could also be due to the fact that the magmatic material of this volcano has a longer residence time in the crust than the rest of the volcanic centers in the southern zone of the Andes.

Finally, the highly resistive R2 is associated with the granitic base Batolito Nor-Patagónico, located in the southeastern part of the Osorno volcano, the Cretaceous base and in the western foot, the Miocene base. The North Patagonian Batolith is mainly formed by granodiorites, diorites, tonalites, granites and

tonalites of hornblende and biotite, mainly igneous rocks that are in the range of resistivity of 1000–100000 Ωm according to Palacky (1987).

6 Conclutions

Based on two and three dimensional inversions of magnetotelluric data in a period range of 10^1 – 10^4S, collected through a profile of 19 sites located between the Central Valley and the Andes mountain range at latitude ~ 41°S, we derived the lithospheric-scale resistivity model of the subduction zone of the Southern Andes.

Different models and dimensional parameters were generated in order to circumvent the effect of the electrical structural anisotropy detected in the data. Data fit is generally good and together with the results of the sensitivity tests we confirmed the robustness of the interpreted model.

The deep electrical resistivity image allowed us to analyze different volcano-detector processes that occur thanks to subduction, in the Southern Zone of the Andes. In our model it was possible to observe the process of serpentinization of the mantle with the early dehydration of the Slab marked as an important decrease of resistivity in the nazca plate at a depth of approximately 50 km, in addition conductive fluids (C1, C2) were observed located in the crust just at the top of where the manetallic wedge should be serpentinizing as a result of the dehydration of the Slab. The location of the conductors under the Central Valley suggests that the release of fluids occurs continuously at different depths during the mineralogical changes presented in the Nazca plate in the development of its subduction.

The position of the large conductor (C3) in the main mountain range is similar to that found by various magnetotelluric studies around the world in subduction zones and which they interpret as a zone of fluid accumulation, generated by a partial fusion related to the phenomenon of eclogitization of the plate that can occur at different depths depending on the degree of hydration or age of the slab.

Other processes of migration and accumulation of fluids through the continental crust were identified in our resistivity image, such as the C5, C6 and C7 anomalies, associated with the Osorno Calbuco volcanoes and the fault systems that dominate the zone. The C5 anomaly that was initially associated with a magmatic chamber located 10 km deep northwest of the Osorno volcano was finally discarded and interpreted as an artifact created by the inversion of the volcanic cone topography.

C6 coincided with the location of a trace of the Liquiñe Ofqui Fault Zone, because of its elongated shape and resistivity values, this anomaly was interpreted as a conduit through which the transport and ascent of fluids is being facilitated and which perhaps communicates with some pre-Andean (Permian - Paleozoic) lineage, belonging to the Andean Transverse Fault system that could be connected in turn to the Calbuco volcano by means of the anomaly (C7), thus explaining the discrepancy between the composition of the lava of the Calbuco and Osorno volcanoes by an apparent differentiation of the magma that has to travel a greater distance and by a different fault system to reach the Calbuco volcanic reservoir.

List Of Abbreviations

Southern Volcanic Zone of the Andes (SVZ),

Liquiñe Ofqui Fault Zone (LOFZ)

Llanquihue Lake (L.LL)

Todos Los Santos Lake (L.TS)

Andean Transverse Fault (ATF)

Magnetotellurics (MT)

magnetic transverse (TM)

electric transverse (TE)

ADU (Analog/Digital Signal Conditioning Unid)

NIMS (Narod Intelligent Magnetotelluric Systems)

Osorno Volcano (VO)

Calbuco Volcano (VC)

Puntiagudo Volcano (VP)

Tronador Volcano (VT)

Declarations

Ethics approval and consent to participate: No applicable

Consent for publication: No applicable

Availability of data and materials: In the following link reviewers can view information supporting the research. Only they can access the data for information purposes. This information is private and cannot be reproduced or modified. This information can only be seen by the reviewers of the paper for information purposes. The information will be published once the article is accepted and published in the journal.

https://osf.io/zsqjc/?view_only=c606c5b2ba7a4991a539630d7e876d5f

Competing interests: We have no conflict of interest in this investigation.

Funding: This research was funded by PIA/CONICYT Anillo ACT-172002 and FONDECYT 1170195.

Authors' contributions: The co-authors supported field data collection, data analysis and geological interpretation of the models.

Acknowledgments: This research was funded by PIA/CONICYT Anillo ACT-172002 and FONDECYT 1170195. We thank the Andean Geothermal Center of Excellence (FONDAP-CEGA, 15090013) for the support with the Metronix equipment used in the field campaigns. We thank Martyn Unsworth and Darcy Cordell (U. Alberta, Canada) for the support with NIMS equipment used for the long period MT data collection. Special thanks to the people who supported the field data collection: Eric Cardenas, Felipe Cordoba, Maria José Hernandez, Miguel Medina, Gustavo Perez, Gabino Reginato and Vicente Yañez. This research was partially supported by the supercomputing infrastructure of the NLHPC (ECM-02).

References

1. Agurto-Detzel, H., Rietbrock, A., Bataille, K. & Miller, M., 2014. Seismicity distribution in the vicinity of the Chile Triple Junction, Aysén Region, southern Chile. Journal of South American Earth Sciences, Volumen 51, pp. 1-11.
2. Angermann, D., Klotz, J. & Reigber, C., 1999. Space-geodetic estimation of the nazca-south america euler vector. Earth and Planetary Science Letters, 171(3), pp. 329-334.
3. Beka, T. I. y otros, 2016. Analysis and 3D inversion of magnetotelluric crooked profile data from central Svalbard for geothermal application. Tectonophysics, Volumen 686, pp. 98-115.
4. Brasse , H. y otros, 2002. The Bolivian Altiplano conductivity anomaly. Journal of Geophysical research, 107(B5), pp. EPM 4-1-EPM 4-14.
5. Brasse, H. & Eydam, D., 2008. Electrical conductivity beneath the Bolivian Orocline andits relation to subduction processes at the South Americancontinental margin. Journal of Geophysical Research, 113(B7).
6. Brasse, H. y otros, 2009. Structural electrical anisotropy in the crust at the South-Central Chilean continental margin as inferred from geomagnetic transfer functions. Physics of the Earth and Planetary Interiors, pp. 7-16.
7. Castruccio, A. y otros, 2016. Eruptive parameters and dynamics of the April 2015 sub-Plinian eruptions of Calbuco volcano (southern Chile). Bulletin of Volcanology, 78(62).
8. Cembrano, J. & Hervé, F., 1993. The Liquine Ofqui fault zone : a major cenozoic strike slip duplex in the Southern Andes. Géodynamique Andine : Symposium International, Volumen 21-23, pp. 175-178.
9. Cembrano, J., Hervé, F. & Lavenu, A., 1996. The Liquine Ofqui fault zone: a long-lived intra-arc fault system in southern Chile. Tectonophysics, Volumen 259, p. 55–66.
10. Cembrano, J. & Lara, L., 2009. The link between volcanism and tectonics in the southern volcanic zone of the Chilean Andes: A review. Tectonophysics, 471(1-2), pp. 96-113.

11. Chang-Hong, L., Han-Dong, T. & Tuo, T., 2011. The possibility of obtaining nearby 3D resistivity estructure from magnetotelluric 2D profile data using 3D inversion. Chinese Journal of Geophysics, 54(1), pp. 72-83.
12. Clemens , J. D. & Mawer, C. K., 1992. Granitic magma transport by fracture propagation. Tecnophysics , Volumen 204, pp. 339-360.
13. Cordell, D. y otros, 2019. Fluid and Melt Pathways in the Central Chilean Subduction Zone Near the 2010 Maule Earthquake (35–36°S) as Inferred From Magnetotelluric Data. Geochemistry, Geophysics, Geosystem, 20(4), pp. 1818-1835.
14. Delgado, F. y otros, 2017. Recent unrest (2002–2015) imaged by space geodesy at the highest risk Chilean volcanoes: Villarrica, Llaima, and Calbuco (Southern Andes). Journal of Volcanology and Geothermal Research, Volumen 344, pp. 270-288.
15. DeShon, H. y otros, 2006. Seismogenic zone structure beneath the Nicoya Peninsula, Costa Rica, from three-dimensional local earthquake P- and S-wave tomography. Geophysical Journal International, 164(1), pp. 109-124.
16. Egbert, G., 1997. Robust multiple-station magnetotelluric data processing. Geophysical journal international, 130(2), p. 475–496.
17. Egbert, G. & Booker, J., 1986. Robust estimation of geomagnetic transfer functions. Geophysical, 87(1), p. 173–194.
18. Egbert, G. & Livelybrooks, D., 1996. Single station magnetotelluric impedance estimation: Coherence weighting and the regression M-estimate. GEOPHYSICS, 61(4), pp. 937-1240.
19. Evans, R., Wannamaker Philip, McGary, S. & Elsenbeck, J., 2014. Electrical structure of the central Cascadia subduction zone: The EMSLAB Lincoln Line revisited. Earth and planetaty science letters, Volumen 402, pp. 265-274.
20. Galanopoulos, D., Sakkas, V., Kosmatos, D. & Lagios, E., 2005. Geoelectric investigation of the Hellenic subduction zone using long period magnetotelluric data. Tectonophysics, 409(1-4), pp. 73-84.
21. Glodny, J., Gräfe, K., Echtler, H. & Rosenau, M., 2008. Mesozoic to Quaternary continental margin dynamics in South-Central Chile (36–42°S): the apatite and zircon fission track perspective. International Journal of Earth Sciences, Volumen 97, pp. 1271-1291.
22. Hervé, F., 1994. The Southern Andes Between 39° and 44°S Latitude: The Geological Signature of a Transpressive Tectonic Regime Related to a Magmatic Arc. Tectonics of the Southern Central Andes, pp. 243-248.
23. Hyndman, R. & Peacock, S., 2003. Serpentinization of the forearc mantle. Earth and Planetary Science Letters, 212(3-4), pp. 417-432.
24. Hyndman, R., Yamano, M. & Oleskevich, D., 1997. The seismogenic zone of subduction thrust faults. Island Arc, 6(3), pp. 244-260.
25. Ichiki, M., Sumitomo, N. & Kagiy, T., 2000. Resistivity structure of high-angle subduction zone in the southern Kyushu district, southwestern Japan. Earth, Planets and Space, 52(8), pp. 539-548.

26. Jiracek, G. R. & Curtis, J. H., 1989. Two-Dimensional Magnetotelluric Inversion of the EMSLAB Lincoln Line. Journal of Geophysical Research, 94(B10), pp. 14,145-14,151.
27. Jödicke, H. y otros, 2006. Fluid release from the subducted Cocos plate and partial melting of the crust deduced from magnetotelluric studies in southern Mexico: Implications for the generation of volcanism and subduction dynamics. Journal of Geophysical research, 111(B8).
28. Jordan, T. E. y otros, 2001. Extension and basin formation in the southern Andes caused by increased convergence rate: A mid-Cenozoic trigger for the Andes. Tectonics, 20(3), pp. 308-324.
29. Kapinos, G., Montahaei, M., Meqbel, N. & Brasse, H., 2016. Three-dimensional electrical resistivity image of the South-Central Chilean subduction zone. Tectonophysics, pp. 76-89.
30. Lange, D. y otros, 2008. First seismic record for intra-arc strike-slip tectonics along the Liquiñe-Ofqui fault zone at the obliquely convergent plate margin of the southern Andes. Tectonophysics, 455(1-4), pp. 14-24.
31. Lavenu, A. & Cembrano, J., 1999. Compressional- and transpressional-stress pattern for Pliocene and Quaternary brittle deformation in fore arc and intra-arc zones (Andes of Central and Southern Chile). Journal of Structural Geology, 21(12), pp. 1669-1691.
32. Leech, M., 2001. Arrested orogenic development: eclogitization, delamination, and tectonic collapse. Earth and Planetary Science Letters, 185(1-2), pp. 149-159.
33. Lopez-Escobar, L. y otros, 1992. A contribution to the petrogenesis of Osomo and Calbuco volcanoes, Southern Andes (41°00'-41°30'S): comparative study. Andean Geology, 19(2).
34. Martí, A., 2014. The Role of Electrical Anisotropy in Magnetotelluric Responses: From Modelling and Dimensionality Analysis to Inversion and Interpretation. Surveys in Geophysics, 35(1), p. 179–218.
35. Mella, M. y otros, 2005. Petrogenesis of the Pleistocene Tronador Volcanic Group, Andean Southern Volcanic Zone. Andean Geology, 32(1), pp. 131-154.
36. Meqbel, N., Weckmann, U., Muños, G., Ritter, O., 2016. Crustal metamorphic fluid flux beneath the dead sea basin: constraints from 2-D and 3-D magnetotelluric modelling. Geophysical Journal International, 207(3), pp. 1609-1629.
37. Moreno, H., Lara, L. & Orozco, G., 2010. Geología del Volcán Osorno, Santiago: Servicio Nacional de Geología y Minería de Chile.
38. Morgado, E. y otros, 2019. Localised heating and intensive magmatic conditions prior to the 22–23 April 2015 Calbuco volcano eruption (Southern Chile). Bulletin of Volcanology, 81(24).
39. Müller, A. & Haak, V., 2004. 3-D modeling of the deep electrical conductivity of Merapi volcano (Central Java): integrating magnetotellurics, induction vectors and the effects of steep topography. Journal of Volcanology and Geothermal Research, 138(3-4), pp. 205-222.
40. Navarro, A., 2019. Caracterización sismotectonica de la cordillera de la costa en Chile Central, entre los 32°30'S y los 34°S, mediante tomografia sismica pasiva, Santiago: Repositorio Académico Universidad de Chile.

41. Palacky, G., 1987. Resistivity characteristics of geologic targets: in Electromagnetic Methods in Applied Geophysics. Nabighian, MN. ed. Tulsa: Society of Exploration Geophysicists.
42. Pankhurst, R., Rapela, C., Fanning, C. & Marquez, M., 2006. Gondwanide continental collision and the origin of Patagonia. Earth-Science Reviews, 76(3-4), pp. 235-257.
43. Patro, P. K. & Egbert, G. D., 2011. Application of 3D inversion to magnetotelluric profile data from the Deccan Volcanic Province of Western India. Physics of the earth and planetary interiors, 187(1-2), pp. 33-46.
44. Peacock, S., 1990. Fluid Processes in Subduction Zones. Science, 248(4953), pp. 329-337.
45. Perez Florez, P. y otros, 2016. Tectonics, magmatism and paleo-fluid distribution in a strike-slip setting: Insights from the northern termination of the Liquiñe–Ofqui fault System, Chile. Tectonophysics, Volumen 680, pp. 192-210.
46. Perez-Florez, P. y otros, 2017. The effect of offset on fracture permeability of rocks from the Southern Andes Volcanic Zone, Chile. Journal of structural Geology, Volumen 104, pp. 142-158.
47. Pommier, A. & Le-Trong, E., 2011. SIGMELTS: A web portal for electrical conductivity calculations in geosciences. Computers&Geosciences, 37(9), pp. 1450-1459.
48. Radic, J. P., 2010. Cenozoic basins and their control on volcanism of Nevados de Chillan and Copahue-Callaqui complexes (36-39°S, Southern Andes. Andean Geology, 37(1), pp. 220-246.
49. Reynard, B., Mibe, K. & Van de Moortele, B., 2011. Electrical conductivity of the serpentinised mantle and fluid flow in subduction zones. Earth and Planetary Science Letters, 307(3-4), pp. 387-394.
50. Rodi, W. & Mackie, R., 2001. Nonlinear conjugate gradients algorithm for 2-D magnetotelluric inversion. GEOPHYSICS, 66(1), p. 174 –187.
51. Saffer, D. M., 2017. Mapping fluids to subduction megathrust locking and slip behavior. Geophysical Research Letters, 44(https://doi.org/10.1002/2017GL075381), p. 9337–9340.
52. Schwalenberg, K., Rath, V. & Haak, V., 2002. Sensitivity studies applied to a two-dimensional resistivity model from the Central Andes. Geophysical Journal International, 150(3), pp. 673-686.
53. Selles, D. & Moreno, H., 2011. Geología del Volcán Calbuco, Santiago: Servicio Nacional de Geología y Minería de Chile.
54. SERNAGEOMIN, s.f. Ministerio de Mineria, Gobierno de Chile, Reporte de actividad volcánica. [En línea]
55. Available at: http://sitiohistorico.sernageomin.cl/lista-region-10.php?pagina=3
56. Shimakawa, Y. & Honkura, Y., 1991. Electrical Conductivity Structure Beneath the Ryukyu Trench-Arc System and Its Relation to the Subduction of the Philippine Sea Plate. Journal of Geomagnetism and geoelectricity, 43(1), pp. 1-20.
57. Slezak, K., Jozwiak, W., Nowozynski, K. & Brasse, H., 2016. 3-D Inversion of MT Data for Imaging Deformation Fronts in NW Poland. Pure and Applied Geophysics, Volumen 173, p. 2423–2434.
58. Smith, T., 1995. Understanding Telluric Distortion Matrices. Geophysical Journal International;, 122(1), p. 219–226.

59. Soyer, W. & Unsworth, M., 2006. Deep electrical structure of the northern Cascadia (British Columbia, Canada) subduction zone: Implications for the distribution of fluids. Geology, 34(1), pp. 53-56.
60. Stesky, R. & Brace, W., 1973. Electrical conductivity of serpentinized rocks to 6 kilobars. Journal of Geophysical Research, 78(32), pp. 7614-7621.
61. Tassara, A. & Echaurren, A., 2012. Anatomy of the Andean subduction zone: three-imensional density model upgraded and compared against global-scale models. Geophysical Journal International, Volumen 189, p. 161–168.
62. Tassara, A. & Yañez, G., 2003. Relación entre el espesor elástico de la litosfera y la segmentación tectónica del margen andino (15-47°S). Revista Geológica de Chile, 30(2), pp. 159-186.
63. Thomson, S. N. & Hervé, F., 2002. New time constraints for the age of metamorphism at the ancestral Pacific Gondwana margin of southern Chile (42-52°S). Revista geológica de Chile, 29(2), pp. 151-165.
64. Völker, D. & Stipp, M., 2015. Water input and water release from the subducting Nazca Plate along southern Central Chile (33°S–46°S). Geochemistry, Geophysics, Geosystems, 16(6), pp. 1825-1847.
65. Vozoff, K., 1991. Electromagnetic methods in applied geophysics - Applications, chapter The magnetotelluric method.. 641-711 ed. s.l.:Society of Exploration Geophysicists II.
66. Wannamaker, P. y otros, 2014. Segmentación del acoplamiento de placa, destino de los fluidos de subducción y modos de magmatismo de arco en Cascadia, inferidos de la resistividad magnetotelúrica. Geochemistry, Geophysics, Geosystems, 15(11), pp. 4230-4253.
67. Wiese, H., 1962. Geomagnetische Tiefentellurik Teil II: Die Streichrichtung der untergrundstrukturen des elektrischen Widerstandes, erschlossen aus geomagnetischen Variationen. Pure and applied geophysics, Volumen 52, pp. 83-103.
68. Worzewski, T. y otros, 2011. Magnetotelluric image of the fluid cycle in the Costa Rican subduction zone. Nature Geoscience, Volumen 4, pp. 108-111.
69. Zuñiga Armijo, F., 2019. Estructuras Magmaticas bajo el Volcán Osorno, identificadas mediante Magnetotelurica, dissertstion, Santiago, Chile: Repositorio Universidad de Chile.

Figures

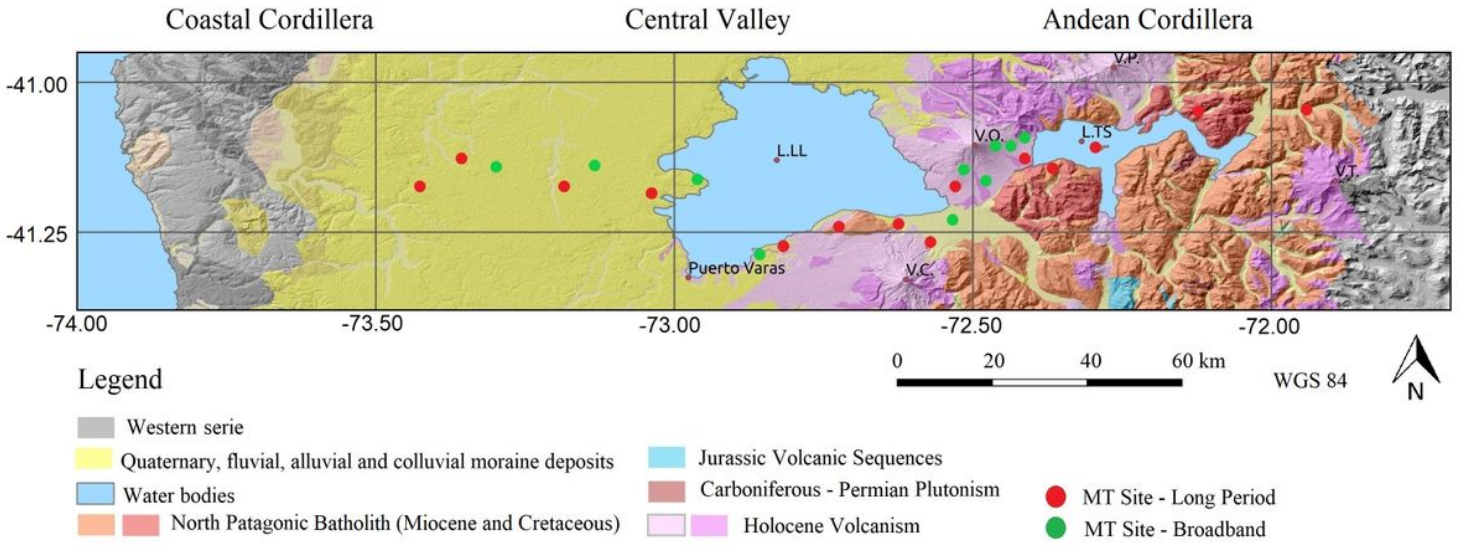

Figure 1

Study area and location of magnetotelluric sites. From west to east, the main morpho-structures that dominate the study zone correspond to the coastal mountain range that dates from the Paleozoic and is made up of the western series, the central valley made up mainly of marine Cenozoic volcanic rocks and glacial sediments and the Andes mountain range where the Nor-Patagonic batholith is developed, made up mainly of alkaline plutonic rocks from the Middle Jurassic to the Miocene. Dotted line represents the trace of the Liquiñe Ofqui fault zone, L.LL Lake Llanquihue, LTS Lake Todos los Santos and VO, VC, VP, VT represents the Osorno, Calbuco, Puntiagudo and Tronador volcanoes respectively.

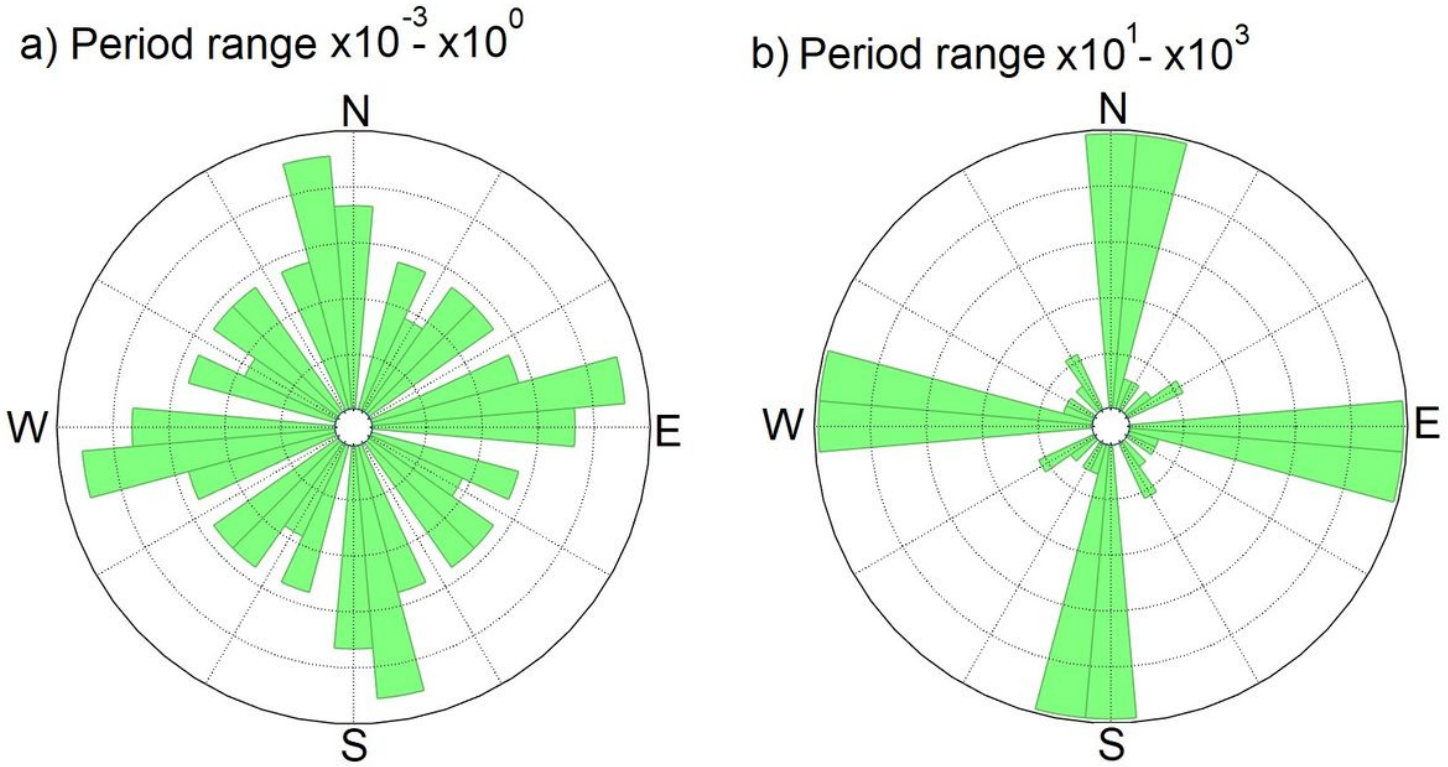

Figure 2

A: Geoelectric strike for different period ranges. a) corresponds to the geoelectric strike for sites with periods between 10-3 and 100. b) corresponds to the geoelectric strike for sites with periods between 101 and 103.

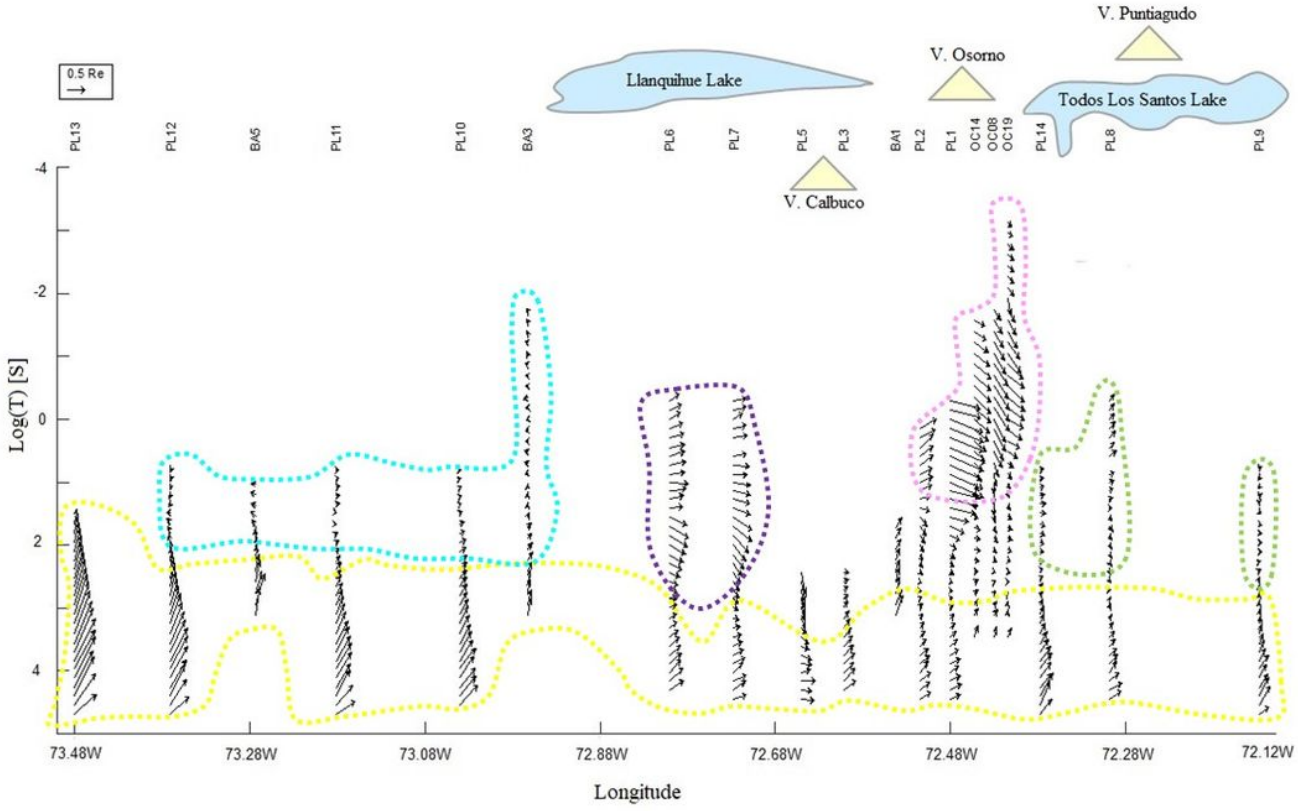

Figure 3

Induction vectors plotted under the convention of (Wiese, 1962), the arrows point in the opposite direction of the conductive zone. The vectors enclosed in the yellow box indicate an anisotropic electrical behavior in the crust, the vectors enclosed by the light blue and green zone, because of their magnitude, could indicate data that are within a conductive body and the vectors enclosed in the purple zone indicate a strong conductor to the west area of the profile, the arrows enclosed by the pink line would be related to a conductor in the Osorno volcano.

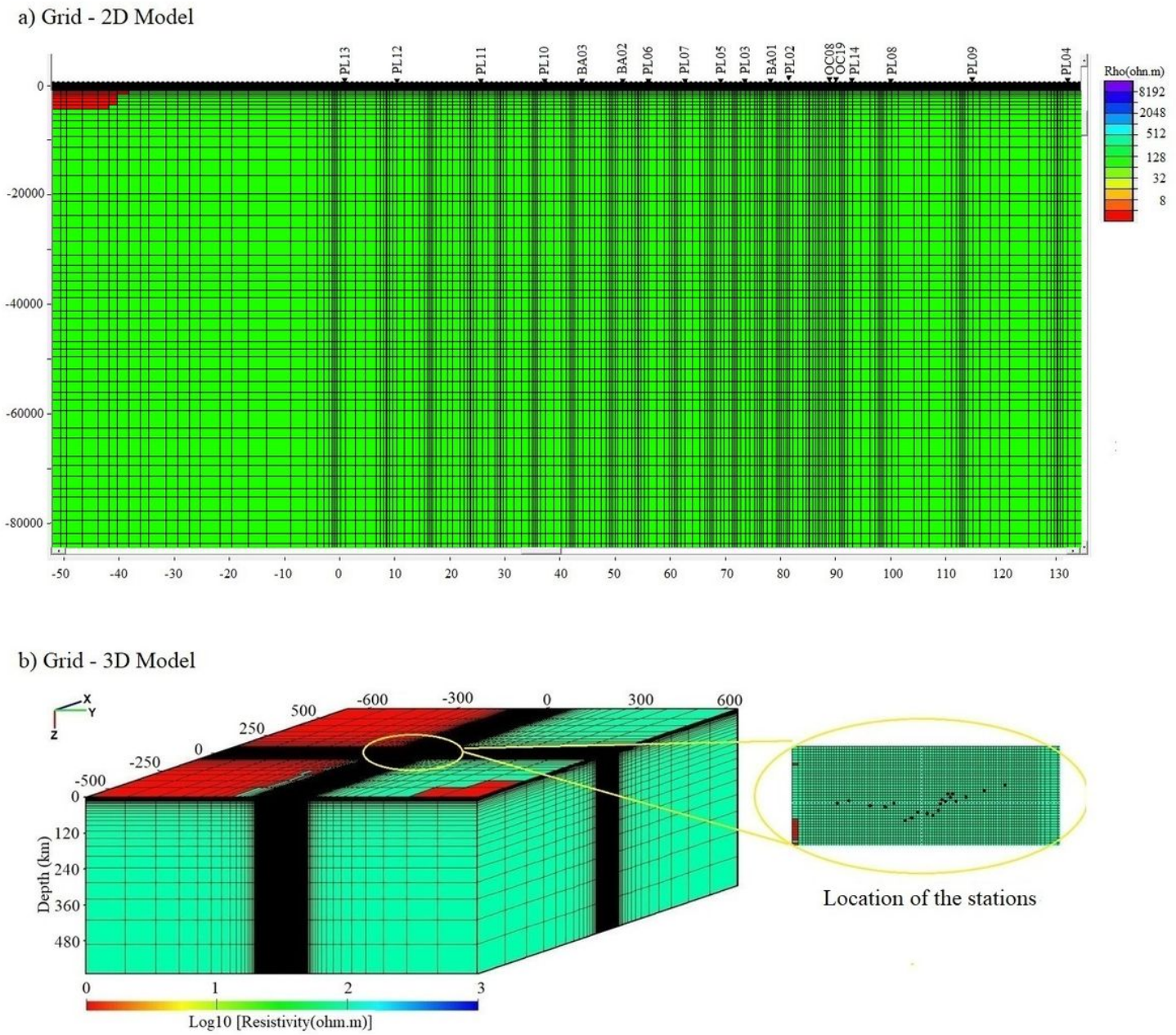

Figure 4

(a) A priori model for two-dimensional model in WinGLink software, the Pacific Ocean (red) 0.3 Ωm and a background resistivity of 100Ωm. (b) Grid construction for 3D inversion. Red cells simulate the presence of the ocean in the initial model.

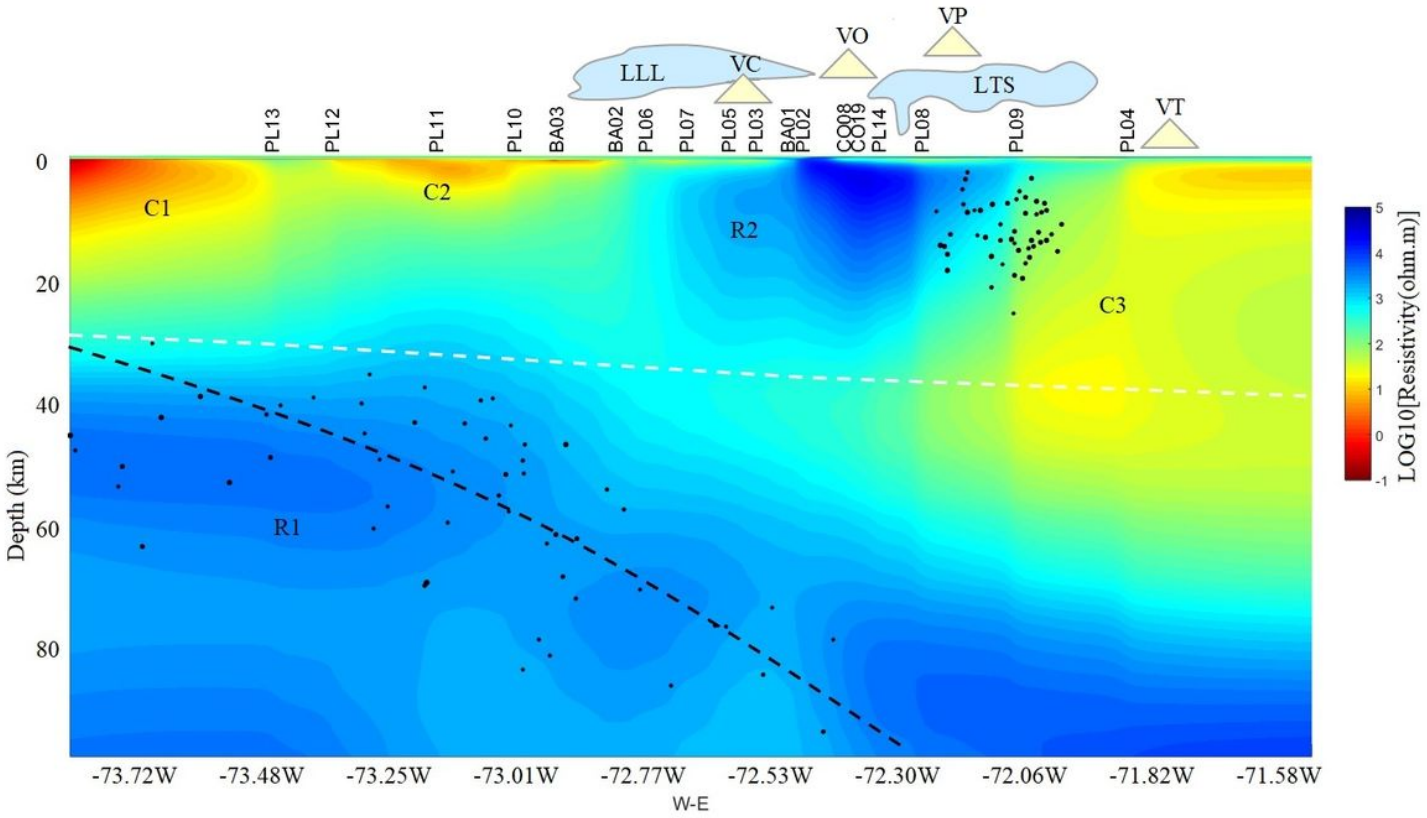

Figure 5

Final two-dimensional model RMS 1.88%. With the local geology of reference, Lago Llanquihue (L.LL), Lago de Todos Los Santos (L.TS), Calbuco (VC), Osorno (VO), Tronador (VT) and Puntiagudo (VP) volcanoes; the black circles correspond to the seismicity of the zone recorded among the 39. 5° and 41.5°S by the Chilean CSN, The white dashed line corresponds to the Moho discontinuity, taken from the Crust1.0 model by (Laske, et al, 2013). The black dashed line refers to the Slab1.0 (Hayes, et al., 2012). C" bodies correspond to conductive structures while "R" bodies correspond to resistive ones.

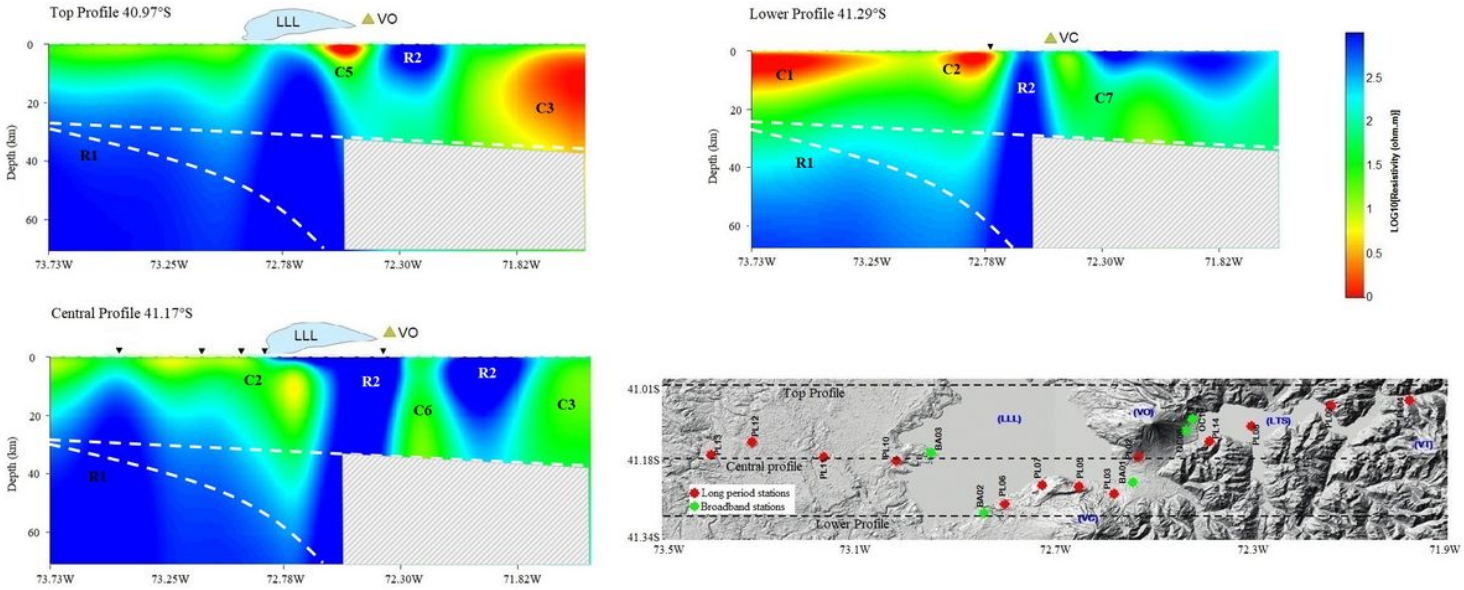

Figure 6

Three-dimensional model RMS 1.95% (a) 3D model profiles. Upper profile 41.02°S, middle profile 41.17°S, lower profile 41.29°S. Location of the profiles shown in (b). Hatched zones are related to poor resolution. (c) Location of 3D model profiles.

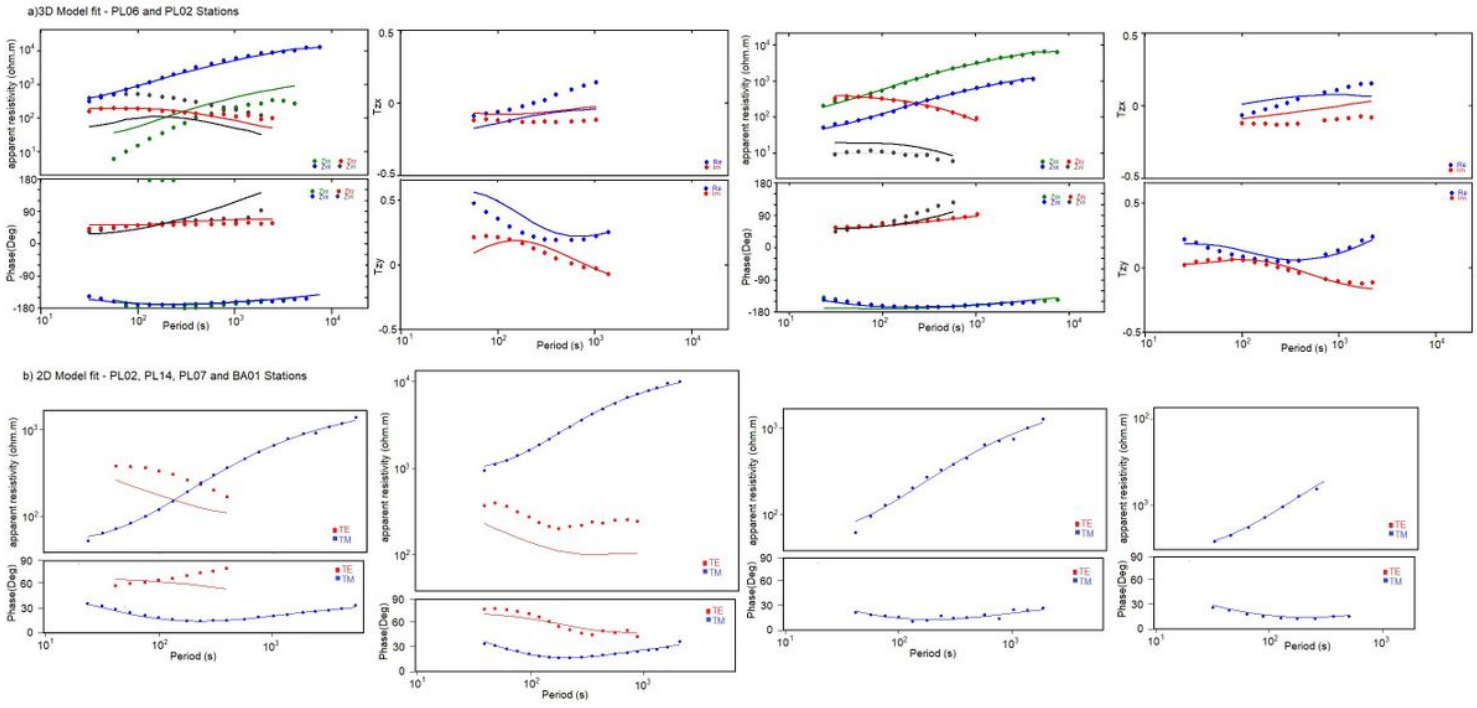

Figure 7

Comparison between measured data (dots) and model response (continuous lines) at four exemplary sites. 2D and 3D model fit curves Best and worst fitting curves.

Supplementary Files

This is a list of supplementary files associated with this preprint. Click to download.

- FigResumen.jpeg